Non-linear Heat Transport Modelling with Edge Localized Modes and Plasma Edge Control in Tokamaks.

M. Bécoulet (1), G. Huysmans(1), P. Thomas(1), P. Ghendrih(1), A. Grosman(1) , P. Monier-Garbet(1), X. Garbet (1),W. Zwingman(1), E. Nardon (1),
R. Moyer (2),
T.Evans(3), A. Leonard (3).

(1)Association Euratom-CEA, CEA Cadarache, F-13108 St. Paul-lez-Durance, France.
(2)University of California, San Diego, La Jolla CA 92093-0417,USA.
(3) General Atomics, 3550 General Atomics Court,P.O.Box 85608 San Diego, CA, USA.

Abstract. The paper presents a new approach for the modelling of the pedestal energy transport in the presence of Type I ELMs based on the linear ideal MHD code MISHKA coupled with the non-linear energy transport code TELM in a realistic tokamak geometry. The main mechanism of increased transport through the External Transport Barrier (ETB) in this model of ELMs is the increased convective flux due to the MHD velocity perturbation and an additional conductive flux due the radial perturbation of the magnetic field leading to a flattening of the pressure profile in the unstable zone. The typical Type I ELM time-cycle including the destabilisation of the ballooning modes leading to the fast (200μs) collapse of the pedestal pressure followed by the edge pressure profile re-building on a diffusive time scale was reproduced numerically. The possible mechanism of Type I ELMs control using a stochastic plasma boundary created by external coils is modelled in the paper. In the stochastic layer the transverse transport is effectively increased by the magnetic field line diffusion. The modelling results for DIII-D experiment on Type I ELM suppression using the external perturbation from the I-coils demonstrated the possibility to decrease the edge pressure gradient just under the ideal ballooning limit, leading to the high confinement regime without Type I ELMs.

1.Introduction

The physics of Edge Localised Mode (ELM) remains one of the important and still unsolved problems for H-mode scenarios in ITER [1]. This motivates present research to combine high plasma confinement with maximum pedestal energy and acceptable heat loads on the ITER divertor target plates during ELMs [2-3]. Type I ELMs are believed to be a manifestation of MHD modes driven by both the steep edge pressure gradient characteristic for the H-mode (ballooning modes) and the edge current, which has a large bootstrap fraction in the region of gradients (peeling modes) [4-5]. ELMs cause the periodic crashes of the pedestal pressure on an MHD time scale (~250μs [6]) followed by the pedestal pressure build-up on a longer diffusive time scale (few ms). The traditional ideal MHD description of ELMs physics permits to analyse a given stationary pressure and edge current profile on peeling-ballooning stability and the calculate linear growth rate of the modes [5,7-9], but the energy and particle transport due to the instability demands a non-linear description. The non-linear approach used here is based on the linear MHD code MISHKA [9] coupled with the non-linear heat transport code TELM described in the present paper. This approach permits the modelling of both pedestal pressure profile relaxations (ELMs) due to destabilisation of ballooning mode by the edge pressure gradient and the transport in the stochastic magnetic field. The main heat transport mechanism in both cases is the additional radial conductive transport appearing the presence of the radial magnetic field perturbation.

2.Theoretical and numerical model

A non-linear energy transport equation:

$$\frac{\partial P}{\partial t} + \vec{\nabla} \bullet \vec{\Gamma} + S_{SOL} = 0 \qquad (2.1)$$

is solved in the pedestal region in realistic tokamak geometry in magnetic flux co-ordinate system $\{s, \theta, \phi\}$with straight magnetic lines ($\psi -$ is a normalised poloidal magnetic flux,

$s=\sqrt{\psi}$, ϕ is toroidal angle and $\frac{d\phi}{d\theta}=q(\psi)$) [9]. Parallel and perpendicular to the magnetic field convective and conductive heat fluxes are taken in the following form: $\vec{\Gamma}=-\chi_{//}\cdot\vec{\nabla}_{//}P-\chi_{\perp}\cdot\vec{\nabla}_{\perp}P+\delta\vec{V}\cdot P$, where δV is MHD velocity perturbation (equal zero in equilibrium), $P=P_0+\delta P$ is a sum of pressure perturbation δP and averaged total plasma pressure $P_0=P_i+P_e$. Here ion and electron pressure are considered to be equal ($P_i=P_e=n_eT_e$) and electron density is taken as constant n_e=const.

The perpendicular transport coefficient $\chi_{\perp}$ is chosen to match the stationary experimental pressure profile in H-mode. In the region of External Transport Barrier (ETB) $\chi_{\perp}$ is reduced to the neoclassical value. The introduction of the conductivity parallel to the magnetic field in the fluid equations implicitly assumes strong collisionality plasmas [10] meaning that electron mean free path $\lambda_{ee}[m]=\frac{1.7310^{17}T^2_{e[eV]}}{n_{e[m^{-3}]}\ln\Lambda}$ is much shorter than the typical parallel gradient scale length $\lambda_{te}<<L_T$. In present modelling the typical length is $L_T\cong\pi Rq/n$, where n is characteristic toroidal wave number of the perturbation. Usually the ratio (collisionality, if n=1) $\nu^*=L_T/\lambda_{te}$ varies strongly in the pedestal region and in particular on the top of the pedestal where $\nu^*<<1$ in a typical H-mode scenario. The use of Spitzer-Härm [10] expression for thermal conductivity $\chi_{//}^{Spitzer}[m^{-1}s^{-1}]=2.10^{22}T^{5/2}_{e[eV]}$ for low collisionality plasmas could lead to unphysical large heat fluxes even at very small parallel gradients. In order to extend the fluid approach various prescriptions were proposed based on comparisons with kinetic analysis for particular problems [10,11]. In present paper we used the kinetic corrections based on the parallel heat flux limit approach from [10]: $\frac{1}{\Gamma_{//}}=\frac{1}{\Gamma_{e,\lim it}}+\frac{1}{\Gamma_{e,Spitzer}}$, where $\Gamma_{e,limit}=\alpha_e n_e v_{te} kT_e$ and α_e is an ad hoc numerical factor adjusting kinetic and fluid modelling results specific for each problem [10,11]. This approach gives the expression: $\chi_{//}=\frac{\chi_{//}^{Spitzer}}{2n_e}\frac{1}{1+(1/\alpha_e)\lambda_{ee}/L_T}$ used in (2.1) with α_e~10^{-2} for a toroidal number n=10 (See Fig.15). The simplified model for the parallel losses in SOL is used:

$$S_{SOL}=\begin{cases}0 & \text{if } s<s_{SOL}\\ \frac{P}{\tau_{//}^{ion}} & \text{if } s\geq s_{SOL}\end{cases}\qquad(2.2)$$

where $\tau_{//}^{ion}=\frac{2\pi Rq_{95}}{C_s}$ is a characteristic energy transport time during Type I ELM from the pedestal to the divertor [12], C_s is the ion sound speed. The position of the separatrix s_{SOL}=0.99 is a parameter in TELM modelling.

The basis vectors perpendicular to the co-ordinate surfaces (s=const, θ=const, ϕ=const) can be represented as: $\vec{a}^1=\vec{\nabla}s;\ \vec{a}^2=\vec{\nabla}\theta;\ \vec{a}^3=\vec{\nabla}\phi$. The co-variant basis vectors used in TELM are : $\vec{a}_1=f\cdot J\cdot\vec{\nabla}\theta\times\vec{\nabla}\phi;\ \vec{a}_2=f\cdot J\cdot\vec{\nabla}\phi\times\vec{\nabla}s;\ \vec{a}_3=f\cdot J\cdot\vec{\nabla}s\times\vec{\nabla}\theta;$ where $J=1/\vec{\nabla}\psi\bullet\vec{\nabla}\theta\times\vec{\nabla}\phi;\ f=2s$. The gradient parallel to the magnetic field direction can be written in the following form:

$$\vec{\nabla}_{//} = \frac{\vec{B}}{|B|}\left(\frac{\vec{B}}{|B|}\bullet\vec{\nabla}\right) = \bar{a}_1\left\{\left(b^{(1)}\right)^2\frac{\partial}{\partial s} + b^{(1)}b^{(2)}\frac{\partial}{\partial\theta} + b^{(1)}b^{(3)}\frac{\partial}{\partial\phi}\right\} +$$
$$+\bar{a}_2\left\{b^{(2)}b^{(1)}\frac{\partial}{\partial s} + (b^{(2)})^2\frac{\partial}{\partial\theta} + b^{(2)}b^{(3)}\frac{\partial}{\partial\phi}\right\} + \tag{2.4}$$
$$+\bar{a}_2\left\{b^{(3)}b^{(1)}\frac{\partial}{\partial s} + b^{(3)}b^{(2)}\frac{\partial}{\partial\theta} + (b^{(3)})^2\frac{\partial}{\partial\phi}\right\};$$

Where $b^{(i)} = \frac{B^i}{|B|}$; $B^i = (\vec{B},\vec{a}^i)$; $i = 1,2,3$; notice that for equilibrium magnetic field: $\vec{B}_0 = \vec{\nabla}\phi\times\vec{\nabla}\psi + I\vec{\nabla}\phi$ the component $B_0^{(1)}$ =0. The perpendicular component of gradient operator is presented as follows:

$$\vec{\nabla}_{\perp} = \vec{\nabla} - \vec{\nabla}_{//} = \vec{a}^1\frac{\partial}{\partial s} + \vec{a}^2\frac{\partial}{\partial\theta} + \vec{a}^3\frac{\partial}{\partial\phi} - \vec{\nabla}_{//}; \tag{2.5}$$

The transport code TELM is a 2D-code, using a finite volume discretisation in the radial (s) and poloidal directions (θ) and a Fourier transform over the toroidal angle (ϕ). The pressure, fluid velocity and magnetic perturbation are presented as:

$$P(s,\theta,\phi) = \sum_{n=\pm\infty} P_n(s,\theta)\cdot e^{in\phi};$$
$$V^{(1,2,3)}(s,\theta,\phi) = \sum_{n=\pm\infty} V_n^{(1,2,3)}(s,\theta)\cdot e^{in\phi};\quad V_0^{(1,2,3)} = 0; \tag{2.6}$$
$$b^{(1)}(s,\theta,\phi) \sim \frac{B^1}{|B_0|} = \sum_{n=\pm\infty} b_n^{(1)}(s,\theta)e^{in\phi};\quad b_0^{(1)} = 0;$$

The condition for incompressible fluid, $\nabla\bullet\vec{V} = 0$, is satisfied exactly in TELM code. The coupling of the toroidal harmonics is taken into account up to the second order of the perturbations to the equilibrium values. In this approximation the expression for radial component of the energy flux can be written as follows:

$$\Gamma_n^1 = \left[-\chi_{\perp}g^{11} - (\chi_{//} - \chi_{\perp})\tilde{\delta}^2\right]\frac{\partial P_n}{\partial s} +$$
$$+\left[-\chi_{\perp}g^{12}\right]\frac{\partial P_n}{\partial\theta} + \left[-(\chi_{//} - \chi_{\perp})b_0^{(2)}\right]\sum_{n'=\pm\infty} b_{-n'}^{(1)}\cdot\frac{\partial P_{n+n'}}{\partial\theta} + \tag{2.7}$$
$$+\left[-i(\chi_{//} - \chi_{\perp})b_0^{(3)}\right]\sum_{n'=\pm\infty} b_{-n'}^{(1)}\cdot(n+n')P_{n+n'}\cdot +$$
$$+\sum_{n'=\pm\infty} V_{-n'}^{(1)}P_{n+n'};$$

Were $\tilde{\delta}^2 = \sum_{n'} b_{n'}^{(1)}\cdot b_{-n'}^{(1)} = \sum_{n'} b_{n'}^{(1)}\cdot(b_{n'}^{(1)})^*$. Notice that $b^{(1)}$ is a dimensional parameter. The convention in the code is n<0, m>0, since on the resonant surface q_{res}=-m/n>0. The cubic non-linear terms in (2.7) are neglected except the coherent one. This term is very important in the averaged pressure profile relaxation (harmonic n=0) since it is coupled with radial gradient $\frac{\partial P_0}{\partial s}$. Since the experimental typical values of the ratio $\chi_{//}/\chi_{\perp} \sim 10^6 >> 1$, even small perturbations of the magnetic field $\delta\vec{B}$ can produce significant transport.

3. Pedestal transport with ELMs

In the case of the heat transport due to Type I ELMs the radial magnetic perturbation and the fluid velocity structure are taken from the MISHKA code modelling for ballooning modes. The ballooning mode is destabilised if the normalised pressure gradient $\alpha = -C_0 \frac{\partial P_0}{\partial s}$ exceeds the critical value. The radial magnetic perturbation of an n=-10 ballooning mode is presented in Fig.1. Plasma parameters and equilibrium were taken for DIII-D shot #115467 during the ELMy H-mode phase [13] and are presented in Fig. 2.

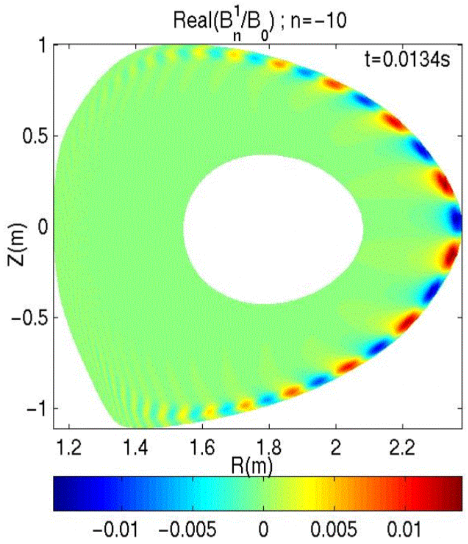

Fig. 1. Magnetic field component perpendicular to the magnetic surface corresponding to the moment of the maximum development of a ballooning mode n=-10.

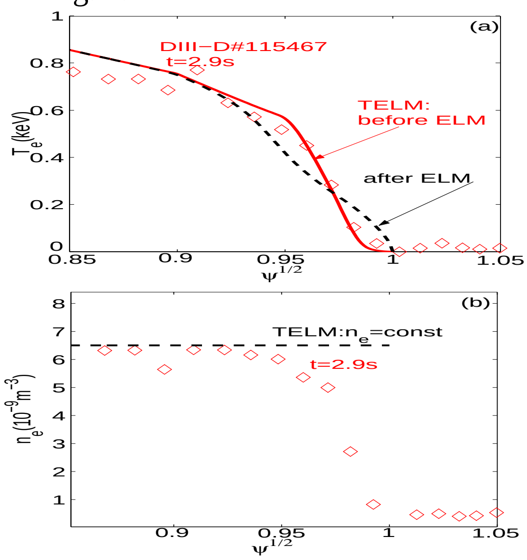

Fig. 2. (a)-electron temperature profiles in experiment [13] and TELM modelling: T_e profile "after" ELM corresponds to the moment of the maximum magnetic perturbation B^1(n=-10) and separated from the profile "before" by 100µs. (b)-electron density profile.

.

The time dependence of MHD perturbations is taken as $\sim e^{\lambda t}$. The linear growth rate λ for MHD mode (here medium n ballooning) on the most unstable magnetic surface (usually corresponding to the maximum pressure gradient) is calculated with the MISHKA code for the initial averaged pressure profile P_0 (t=0,s) and then linearly extrapolated for the averaged pressure P_0(t,s) which evolves in time due to the transport generated by the unstable mode:

$$\lambda = \begin{cases} \lambda_1 = C_1\sqrt{(\alpha - \alpha_{crit})} & \text{if} \quad \alpha > \alpha_{crit}; \\ \lambda_2 = -\Delta & \text{if} \quad \alpha < \alpha_{crit}; \end{cases}$$
$$\alpha = C_2 \frac{\partial P_0(t)}{\partial s}; \qquad C_2 = \frac{\alpha_{eq}}{\dfrac{\partial P_0(t=0)}{\partial s}} \tag{3.1}$$

The constants $C_{0,}$ C_1 and C_2 are calculated by the MISHKA code for a given equilibrium and toroidal harmonic number n. The normalised pressure gradient α and the marginally stable pressure gradient α_{crit} is calculated for the most unstable surface (here s=0.97). This approximation is justified by MISHKA calculations where the λ^2 dependences on α and toroidal number n are almost linear. The growth rate λ is positive for growing ideal modes when normalized pressure gradient $\alpha > \alpha_{crit}$ and negative when pressure gradient is below the critical value and represents the damping level ($\Delta > 0$). In the simulations we use values of Δ

to adjust experimental ELM time. The time evolution of the pedestal pressure (a), fluid velocity (b), magnetic perturbation (c) and radial flux through separatrix (here s=0.99) during an ELM are presented ion Fig.3 and Fig.4.

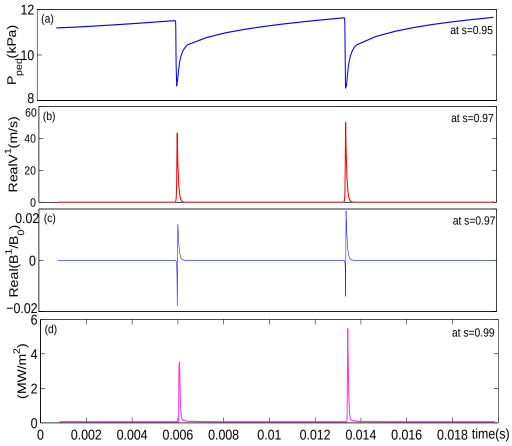

Fig. 3. (a)- Pedestal pressure(at s=0.95), (b)- radial velocity $V^1 = (\vec{V}, \nabla s)$ at s=0.97, θ=0; (c)-radial magnetic field at s=0.97, θ=0; (d)- averaged radial heat flux Γ^1_0 at s=0.99.

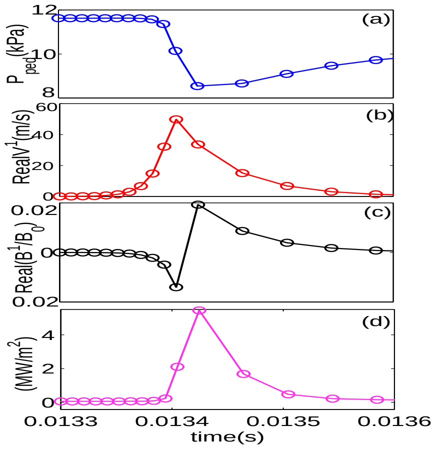

Fig. 4. Zoom of Fig.3 for a second ELM.

The results of the simulations demonstrated the compatibility of the model and the main experimentally observed characteristics of Type I ELMs: the ballooning structure, the fast collapse of the pressure profile on a MHD time scale (ELM time ~200µs) and the pressure profile re-building on a diffusive time scale (here ~8ms). The pedestal transport is increased significantly when MHD mode is destabilized due to the increased convective flux and an additional conductive flux due to the radial perturbation of the magnetic field (see 2.7) both leading to a flattening of the pressure profile in the unstable zone (Fig.2a). However the present model of Type I ELMs has obvious simplifications and ad hoc parameters (see Sec.2) limiting the realistic description of the energy loss in ELM. In particular the simplified model for the parallel losses in the SOL (2.2) does not include any description of the non-linear phase and possible reconnections of the perturbed magnetic field lines and open field lines in the SOL.

4.Modelling of ELMs control by stochastic fields. The present version of the pedestal heat transport model includes the possibility to calculate the effect of the magnetic perturbation generated by external coils. It was demonstrated theoretically and experimentally that a small radial perturbation of the magnetic field can induce chaotic behaviour of the magnetic field lines. In this case the radial diffusive heat transport is amplified by the diffusion of the magnetic field lines in the ergodic zone [15-17].

The experiment of Type I ELM suppression by I-coils on DIII-D [13] was taken as an example for modelling in the present paper. The set of six upper and lower I-coils is presented in Fig.5. A static magnetic perturbation was calculated using Biot-Savart law for the experimental set-up described in [13], which was the alternative current feeding of the current loops in poloidal direction and asymmetric with respect to the mid plane z=0. The mid-plane view of the cylindrical radial component of the magnetic field is shown Fig.6. The main toroidal harmonic number is n=3. The poloidal view of the harmonic n=3 is presented in Fig.7. The poloidal view of the perpendicular component, $B^{(1)} = (\vec{B}, \nabla s) = B_R \frac{\partial s}{\partial R} + B_z \frac{\partial s}{\partial z}$, is presented in Fig.8 and Fig.9 for a realistic experimental value of the coil current I_{coil}=4kA. The units on Fig. 8-9 are arbitrary: all lengths are normalised to the major radius (R_M=1.77m) and magnetic field is normalised to the value on axis (B_M=1.6T). The poloidal spectrum of $b^{(1)}_n$ in magnetic flux coordinates is peaked at the poloidal mode number m=10 for the ψ=1 and m=8 at the ψ=0.95 surfaces (Fig.10).

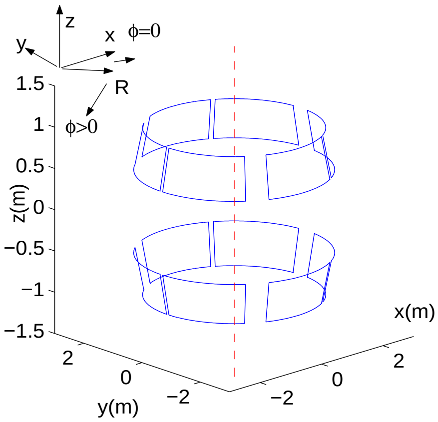

Fig. 5. I-coils geometry .

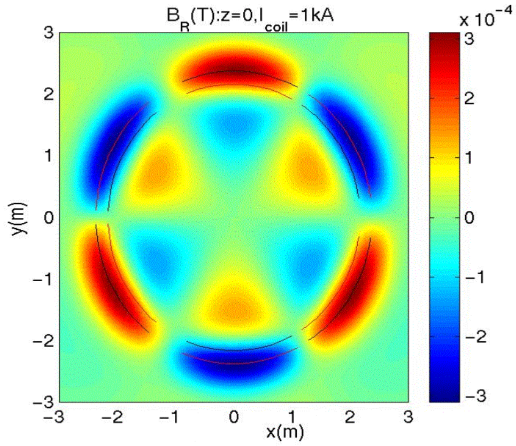

Fig. 6. Radial cylindrical component of the magnetic field generated by a set of I-coils in DIII-D at I=1kA.

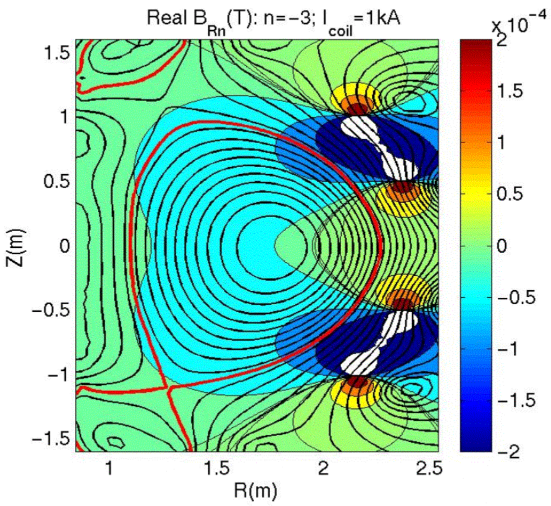

Fig.7. Harmonic n=3 of the radial cylindrical component of the magnetic field at I=1kA.

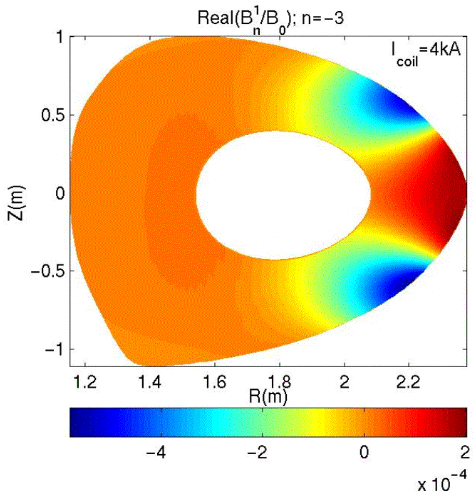

Fig. 8. Real($B_n^{(1)}/B_0$). Ratio of the radial magnetic perturbation harmonic n=-3 to the equilibrium field in TELM a.u. for I=4kA.

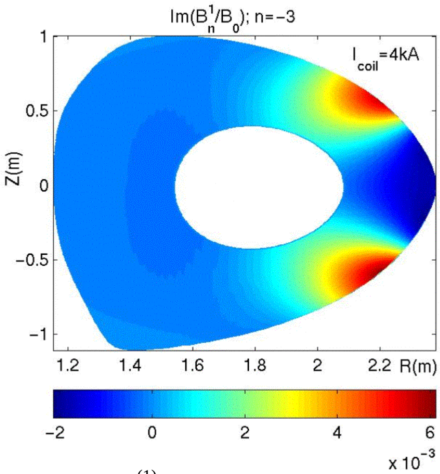

Fig. 9. Im ($B_n^{(1)}/B_0$) in TELM a.u. for I=4kA.

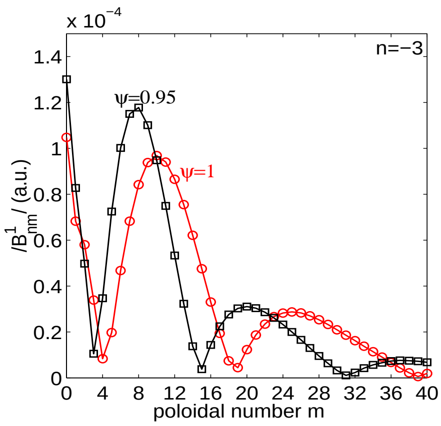

Fig.10. Poloidal spectrum of the magnetic perturbation (I_{coil}=1kA).

. The radial profiles for the different poloidal harmonics are presented in Fig.11. The resonant surfaces are represented by vertical dashed lines. Since the I-coils were not initially designed for the ergodisation of the edge, the perturbation is not maximum at the edge for this magnetic configuration TELM modelling demonstrated a island-like structure of the pressure perurbation situated near the top of the pedestal with a characteristic poloidal number m~9 (Fig.12).

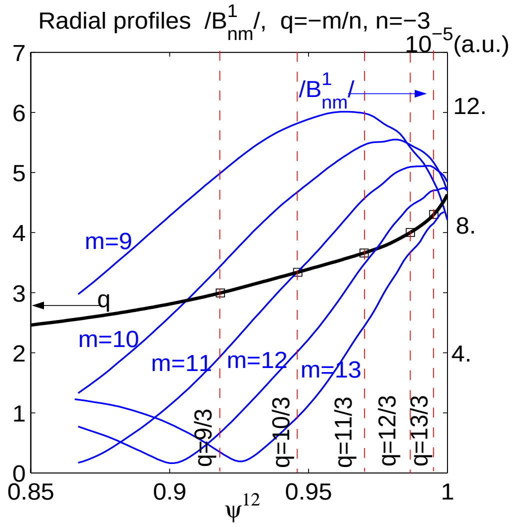

Fig. 11. Radial dependence of $/B^1{}_{mn}/$ harmonics for the spectrum presented in Fig.10 (I_{coil}=1kA)

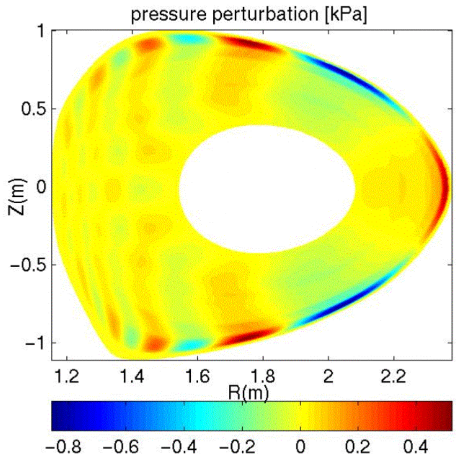

Fig. 12. Islands structure on the pressure perturbation from TELM modelling of DIII-D shot #115467 with I-coils current ~4kA.

.

The simulated profiles with and without ELMs are in the error bars of the experimental values (Fig.14). The effective increase in the perpendicular heat diffusivity due to the radial perturbation of the magnetic field can be estimated from the expression (2.7) for the averaged perpendicular flux $\Gamma_0^1 \sim -(\chi_\perp + \chi_{//}\frac{\tilde{\delta}^2}{g^{11}})g^{11}\frac{\partial P_0}{\partial s}$. The transport coefficients used in modelling are presented in Fig.15.

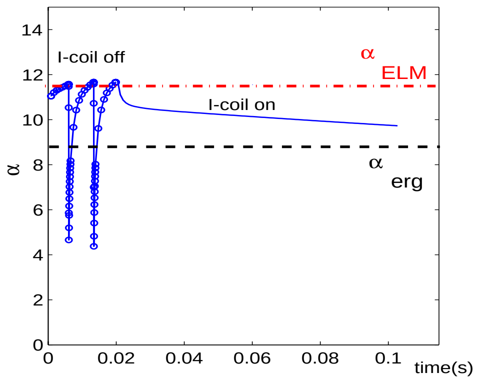

Fig. 13. Normalised pressure gradient reaches critical value (α_{ELM}) for ELM triggering at I_{coil}=0 and remains just under with I_{coil}=4kA

The electron pressure profiles and hence plasma confinement are almost the same during the ELMy phase and when the ELMs are suppressed by the I-coils [13]. The modelling results indicate that during the stationary phase without ELMs the confinement in the pedestal is just marginally degraded and the critical pressure gradient is not reached, resulting in the suppression of ELMs in numerical simulations (Fig.13). This result is proposed as one of the possible explanations of the observed experimental facts. It still requires further experimental confirmation, since all numerical profiles with and without ELMs are in the error bars of the experimental values (Fig.14).

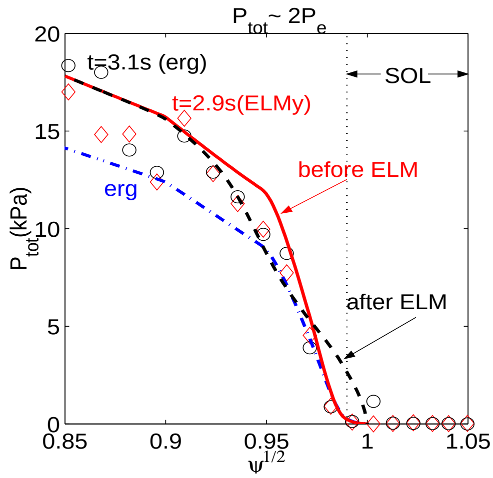

Fig.14. Experimental and numerical total averaged pressure profiles with ("ELMy") and without ELMs ("erg") for DIII-D shot #115467.

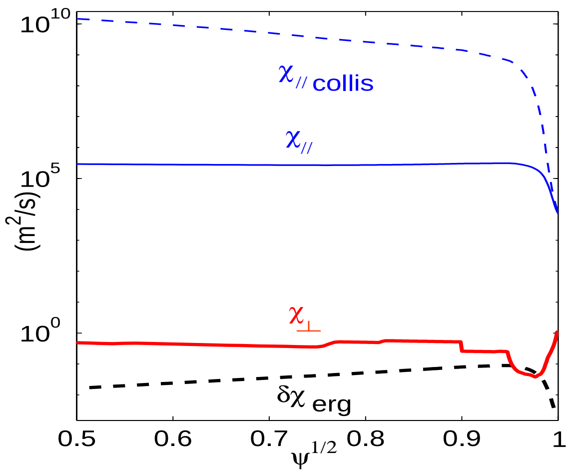

Fig.15. Characteristic parallel and perpendicular diffusivities used in modelling:
$\chi_{//\,\mathrm{collis}} = \frac{\chi_{//}^{\mathrm{Spitzer}}}{2n_e}$; $\chi_{//} = \frac{\chi_{//}^{\mathrm{Spitzer}}}{2n_e} \frac{1}{1+(1/\alpha_e)\lambda_{ee}/L_T}$
Effective poloidal angle averaged ergodic coefficient is estimated as follows: $\delta\chi_{\mathrm{erg}} = \chi_{//} \frac{\tilde{\delta}^2}{<g^{11}>_\theta}$;

5. Conclusions.

The 2D code TELM has been developed for the modelling of the pedestal transport in the presence of small radial perturbations of the magnetic field and small displacements of the magnetic surfaces. Periodic relaxations of the pedestal pressure due to the destabilisation of ballooning modes reproduce the main experimental features of Type I ELMs: the ballooning character of the crash on the outboard of the tokamak, the fast MHD time scale for the temperature collapse and the diffusive time scale for recovery phase. The modelling of the influence of the external magnetic perturbation demonstrated the possibility of the control of Type I ELMs using a stochastic plasma boundary created by the external coils without significant loss of plasma confinement.

References:

[1] BJ Green for the ITER Int. Team, Plasma Phys. Control. Fusion, **45** (2003)687
[2] G Federici et al Plasma Phys Control Fus **45** (2003) 1523
[3] A Loarte et al., Plasma Phys Control Fus **45** (2003) 1549
[4] JW Connor, Plasma Phys Control Fus **40** (1998) 531
[5] Snyder P B et al "ELMs and constrains on the H-mode pedestal: a model based on peeling-ballooning modes", Proc. 19th Int. conference (Lyon,2002) (Vienna: IAEA).
[6] M Becoulet, et al., Plasma Phys Control Fus **45** (2003) A93
[7] HR Wilson et al Phys Plasmas **9** (2002) 1277
[8] LL Lao Plasma Phys. Control. Fusion **42** (2000) A51
[9] GTA Huysmans et al Nucl. Fusion 38(1998)179
[10] P C Stangeby, The plasma Boundary of Magnetic Fusion Devices, Plasma Physics Series, IOP Publishing Ltd 2000.
[11] LLE Review 48(1991)181.
[12] T Eich et al J. Nucl. Mater. 313–316 (2003) 919
[13] T Evans et al Phys. Rev. Lett. 92(2004)
[14] AB Rochester and MN Rosenbluth Phys Rev Lett **40**(1978)38A Samain et al Phys Fluids **B5**(1993)471
[15] P Ghendrih et al Plasma Phys. Control. Fusion, **38** (1996)1653
[16] SJ Fielding, RJ Buttery et al., Proc 2001 EPS Conf., ECA, **25A** (2001) 1825